POLITECNICO
MILANO 1863

SCHOOL OF INDUSTRIAL AND
INFORMATION ENGINEERING

Master of Science in Aeronautical
Engineering

Fluid dynamics optimization for the surgical treatment of septal deviations

Advisor: Prof. Maurizio Quadrio

Co-advisor: Prof. Matteo Trimarchi
Ing. Andrea Schillaci
Dott. Umberto Tanzini

Master Thesis by:
Marcello Macellari
941214

Anno Accademico 2020/2021

POLITECNICO
MILANO 1863

SCUOLA DI INGEGNERIA INDUSTRIALE
E DELL'INFORMAZIONE

Executive Summary of the Thesis

Fluid dynamics optimization for the surgical treatment of septal deviations

Laurea Magistrale in Aeronautical Engineering - Ingegneria Aeronautica

Author: Marcello Macellari

Advisor: Prof. Maurizio Quadrio

Co-advisors: Prof. Matteo Trimarchi, Ing. Andrea Schillaci, Dott. Umberto Tanzini

Academic year: 2020-2021

1. Introduction

When severe septal deviations cause relevant obstructions of the nasal airways, ear-nose-throat (ENT) specialists are required to surgically correct them in order to relieve patients' discomfort. Septoplasty, however, has a low success rate, below 80%, when the actual post-operative benefits are considered. As a matter of fact, this inefficiency has to be ascribed to the lack of a standardized and patient-specific method that effectively evaluates septal deviations providing surgeons with information they can use in the surgical planning [1].
In recent years, trying to solve this issue, Computational Fluid Dynamics (CFD) has become one of the most valuable tools to study the details of the nasal airflow, measure its characteristics and relate them with the local anatomy. As a consequence, several works that address different aspects of the application of CFD to this field are present in literature. These studies range from the numerical analysis of the behavior of the nasal airflow to the investigation of the effects of septoplasties that are virtually performed. However, even though extremely valuable, all these works still rely on the subjective interpretation of CFD results thus not providing standardized and reproducible data.
This work lays the foundation for the introduction of a patient-specific and reliable instrument that can support ENT surgeons in the planning of septoplasties. The main idea behind this tool is the integration, in the CFD study of the nasal airflow, of the adjoint formulation that is used to compute sensitivity derivatives for a shape optimization problem. The final outcome of the procedure is a surface sensitivity map which shows if and how much the displacement of a point of the nasal surface is favorable for the minimization of a cost function that indirectly accounts for viscous losses. The robustness of the procedure was tested with its application on three different anatomies. Results were analyzed and validated by surgeons and the possibility of obtaining actual benefits was proved performing a morphing of the geometry, in accordance with the sensitivity map, and computing the new flow characteristics.

2. Methods

The method herein proposed hinges upon the adjoint formulation. However, in order to use it for the computation of the surface sensitivity maps three preliminary steps are needed. These

phases are: (1) the reconstruction of the three-dimensional nasal geometry from available CT scans, (2) the generation of the computational mesh and (3) the simulation of the nasal airflow. The visualization and the elaboration of CT scans was performed using the open-source software 3D Slicer. The reconstruction of the three-dimensional geometries was obtained through the image segmentation process available in the *Segment Editor* module applying a segmentation threshold equal to -475HU. With this procedure, all pixels of the CT image with a radiodensity higher than -475HU were marked as solid boundaries that did not contain air. The remaining points, instead, defined the actual region where the airflow was present. The resulting three-dimensional model was exported and saved in a STereoLitography (STL) format.
The STL file was subsequently used as the main input for the generation of the computational mesh. This phase was performed with `snappyHexMesh`, a tool available in OpenFOAM. An additional STL file was created to simulate the external environment. This was a small sphere, with a diameter of 70mm that was placed in front of the reconstructed geometry with the care of leaving no openings between them. Using both STL files it was possible to obtain the needed computational grids such as the one shown in Figure 1.

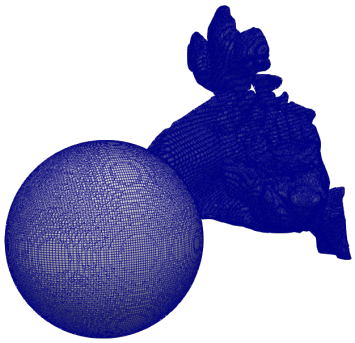

Figure 1: Final computational mesh for one of the patients

Here, it can be noted that finer cells were used for the nasal airways whereas a coarser mesh was defined for the inlet sphere. No layers were added in either of these regions. Table 1 summarizes the main characteristics of the meshes generated for the three selected patients. In all cases more than 5 million elements have been obtained for the inner mesh whereas around 1 million cells characterize the boundaries of the anatomies of the three patients.

	Number of cells	
	Total Mesh	Solid Boundary
P1	5262788	950327
P2	5695738	1052087
P3	6623922	1178278

Table 1: Characteristics of the meshes for the three patients under analysis

After the generation of the meshes, the nasal airflow simulation was set up. For this phase, the flow solver `simpleFoam` was used. The nasal airflow was modeled as a stationary, turbulent and incompressible flow with a given constant flow rate of 15 l/min. All modeling choices were made referring to existing works available in literature [2] [3]. Reynolds-Averaged Navier-Stokes (RANS) equations were solved to guarantee mass and momentum conservation and their closure was ensured with the k-ω SST model. On the boundaries of the reconstructed geometry the no-slip and the no-penetration conditions were enforced for the velocity field **u** whereas the zero gradient was applied for pressure p. At the inlet, the value of **u** was set to ensure the selected flow rate, whereas the zero gradient was, once again, applied for p. At the outlet the zero gradient was enforced for **u** and a value of pressure equal to zero was specified. For the turbulent quantities wall functions were used.

2.1. Adjoint formulation

With the computation of the results of the RANS equations it was possible to start the computation of the surface sensitivity map. To this extent all the elements of the underlying shape optimization problem were specified. The cost function was defined in terms of dissipated power since this quantity was thought to be representative of the resistance that the airflow may encounter in the nasal cavities. In particular, it was specified in terms of net mechanical energy flux through the boundary Γ of the geometry and not directly as viscous losses. Indeed, even though these two quantities give the same values this choice was made to obtain and easier

expression for the cost function written as:

$$f = \int_{\Gamma} d\Gamma (p + \frac{1}{2}u^2)\mathbf{u} \cdot \mathbf{n} \tag{1}$$

It can be noted that f depends only on the flow field variables $\mathbf{u}$ and p. Therefore, since these quantities must always satisfy mass and momentum conservation the constraints of the optimization problem were specialized as the Navier-Stokes equations. At this point, the adjoint formulation was used to compute the sensitivities of this function with respect to the displacements of all points of the nasal walls that were chosen as control variables. Indeed these quantities are the ones that represent what ENT specialists can actually perform during surgeries. The adjoint formulation was preferred over other analytical tools given the huge number of control variables involved. Indeed, for each geometry, these are equal to the number of solid boundary elements reported in Table 1. The adjoint procedure is able to compute all sensitivities at the same time by solving a system of two PDEs. Other formulations, by contrast, would have considered the control variables one by one resulting in an unmanageable computational cost. The adjoint formulation herein developed was derived from the one specialized for ducted flow and defined by Othmer [4].
At the end of all mathematical derivations, the peculiar expression that was obtain for the surface sensitivity was written as:

$$\frac{\partial f}{\partial \beta_i} \propto \mathbf{v}^i \cdot \mathbf{u}^i \tag{2}$$

where β_i is the displacement normal to the surface of cell i and $\mathbf{v}$ is the so-called adjoint velocity. This quantity can be seen, along with the adjoint pressure q, as the Lagrangian multiplier that is introduced when the cost function is studied considering its four constraints. Then, the variation of $\mathbf{v}$ is given by the adjoint equations that, in this work, were written as:

$$\nabla \cdot \mathbf{v} = 0 \tag{3}$$

$$-\nabla \mathbf{v} \cdot \mathbf{u} - (\mathbf{u} \cdot \nabla)\mathbf{v} = -\nabla q + \nabla \cdot (2\nu \mathbf{D}(\mathbf{u})) \tag{4}$$

where $2\mathbf{D}(\mathbf{u}) = (\nabla \mathbf{u} + (\nabla \mathbf{u})^T)$. It should be noted that for the derivation of these equations the *frozen turbulence* hypothesis was used. As such, variations of turbulence quantities with respect to the design variables were neglected and there was no need of deriving the adjoint counterpart of the equations of the k-ω SST model. With the specification of boundary conditions it was then possible to solve these equations, obtain the results for $\mathbf{v}$ and compute the surface sensitivity values. In practice, all these operations were performed using a solver implemented in OpenFOAM. At the inlet and at the solid walls the same conditions of p and $\mathbf{u}$ were applied respectively for q and $\mathbf{v}$. At the outlet, instead, conditions were given by two expressions written as:

$$q = \mathbf{v} \cdot \mathbf{u} + v_n u_n + \nu(\mathbf{n} \cdot \nabla)v_n - \frac{1}{2}u^2 - u_n^2 \tag{5}$$

$$0 = u_n(\mathbf{v}_t - \mathbf{u}_t) + \nu(\mathbf{n} \cdot \nabla)v_t \tag{6}$$

where the subscripts n and t denote the normal and the tangential components.

3. Results

All results were found to be independent with respect to the spatial discretization that was adopted. In particular, grid independence was verified for all patients comparing the overall trends of the surface sensitivity map.
In the following, for the sake of clarity and brevity only the adjoint results obtained for the patient that was identified as the most critical one are reported in full. Nevertheless, also a brief review of the outcomes obtained for $\mathbf{u}$ and p is proposed to highlight the main influences of septal deviations.
Indeed, from the results of the RANS equations, two main features, related to the anatomical anomalies, were observed. First, it was possible to highlight relevant recirculating regions behind septal deviations of the anterior cartilaginous part where air reached low velocity values comparable to the ones of the external environment. Second, in correspondence of narrow restrictions, major pressure drops and considerable velocity picks were obtained. Overall these two characteristics result in a strong asymmetry of the flow field between the two nasal fossae. Table 2 reports, for all three patients, values of flow partitioning and nasal resistance, two of the most relevant quantities for evaluating obstructions.

	Flow partitioning		
	Left cavity	Right cavity	Resistance
	%	%	$Pa/(ml/s)$
P1	32.49%	67.51%	0.091
P2	62.18%	37.82%	0.360
P3	22.93%	77.07%	0.037

Table 2: Flow partitioning and nasal resistance computed for the three anatomies

3.1. Adjoint results

Concerning the adjoint results obtained for the aforementioned patient they are reported in Figure 2 and in Figure 3. These outcomes are visualized in terms of normalized sensitivity values and are rendered on a red scale. All red points are favorable to the minimization of the cost function if displaced in the outward direction with respect to the fluid. All gray points, instead, do not bring any benefit if modified.
Figure 2 shows the surface sensitivity map obtained in correspondence of the left anterior deviation of the patient. On top, it is possible to observe the actual location of the anomaly whereas below a zoomed-in view on the critical region is provided.

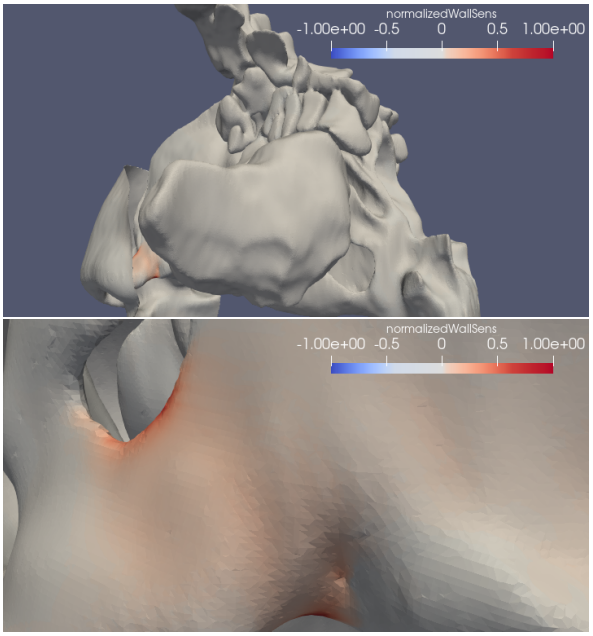

Figure 2: Surface sensitivity map. On top, left lateral view. Below, zoom on the anterior deviation

In this case, the adjoint formulation would suggest to operate on the entire cross-sectional area and not only precisely on the deviation. Nevertheless, as expected, higher normalized sensitivity values around 0.2 can be observed in correspondence of the actual obstruction, i.e. in the top part of the red region. This characteristic would suggest that a more relevant displacement is needed in this part.
Figure 3, instead, shows the outcome obtained for the two restrictions caused by a prominent right bone spur that bridges the entire middle meatus reaching both the inferior and the middle turbinate. As in the previous case both a global lateral view to locate the anomalies and a zoomed-in view on them are provided.

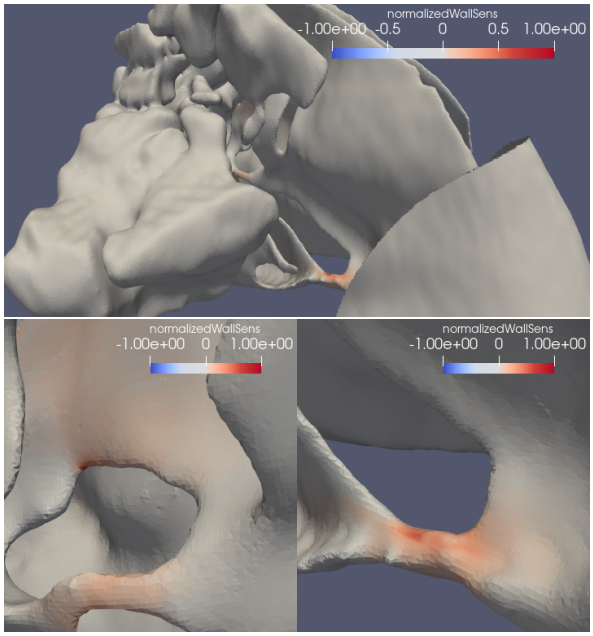

Figure 3: Surface sensitivity map. On top, right lateral view. Below, zoomed-in views on the two restrictions caused by the right bone spur

In correspondence of both restrictions the adjoint formulation would suggest to widen the area even though higher normalized sensitivity values can be observed for the inferior deviation. Here a major contribution for the minimization of the dissipated power can be obtained with an upward displacement of the cells on top of the restriction that have values around 0.4. Considering the other deviation, instead, it is possible to observe that the adjoint formulation would suggest to operate in two different points: one in correspondence of the middle meatus and one that coincides with the part of the right nasal

fossa compressed in between the deviated septum and the middle turbinate.

4. Discussion

An innovative CFD adjoint procedure developed to help ENT surgeons in the planning of septoplasty has been described. The preliminary three steps of this method, preceding the adjoint computation, are usual phases of any CFD study of the nasal airflow and, herein, they were designed to result in a linear sequence of operations. In this regard, it has to be noted that both the chosen segmentation threshold, equal to -475HU, and the idea of representing the external environment with a small inlet sphere were proven to give reliable and valid results, thus providing non-trivial advancements with respect to existing works. In particular, the possibility of obtaining high quality results without the need of using a wide box that entirely surrounds the reconstructed head of the patient in the simulation of the outside air would represent an important saving in terms of computational cost.
Nevertheless, the most critical step of the procedure is the application of the adjoint-based optimization theory to deal with septal deviations. In the previous section, the results obtained with its application for one of the analyzed patients have been provided. These outcomes, along with the ones obtained for the other two anatomies that produced similar conclusions, were reviewed and analyzed by surgeons who confirmed that the adjoint formulation has been able to highlight all septal deviations that might be identified during a routine pre-operative study of the CT scans. Furthermore, from a qualitative point of view the validity of all the results was confirmed by two aspects of the surface sensitivity map: (1) the strong asymmetry between the two nasal fossae that recalled the one of the flow field variables and (2) the essentially null sensitivity values computed in correspondence of paranasal sinuses, turbinates and nasopharynx. From a quantitative standpoint, instead, the peculiar displacements identified by the adjoint formulation were also validated by surgeons who confirmed that all suggested displacements are feasible and usually performed. ENT specialists stressed that the clear advantage in surgical planning with this kind of visualization is that they can easily identify the most relevant parts by looking at the 3D reconstruction, without taking into account specific physical quantities that are often unintuitive.
From a CFD standpoint the derived adjoint formulation was demonstrated to be robust both with respect to the flow model that is used and with respect to the peculiar turbulence model that is adopted for the RANS equations. Indeed, variations in the normalized sensitivity values smaller than 1% were obtained when comparing the results computed with the k-ω SST model with the ones resulting from the application of the k-ϵ or the v^2-f.
Table 3 proves the validity of the procedure by showing the flow partitioning and the nasal resistance computed for the three anatomies modified according to the normalized sensitivity map multiplied by $1mm$.

	Flow partitioning		
	Left cavity %	Right cavity %	Resistance $Pa/(ml/s)$
P1	32.25%	67.75%	0.081
P2	60.63%	39.37%	0.311
P3	23.52%	76.48%	0.033

Table 3: Flow partitioning and nasal resistance values after morphing

For all three patients relevant improvements can be observed in terms of nasal resistance with a relative reduction that is above 10%. Concerning flow partitioning instead, a rebalancing between the two nasal fossae can be noticed for P2 and P3 whereas a minor worsening, smaller than 0.3% is computed for P1. In this regard, it should be noted that the presented procedure, with the displacement set to $1mm$, is not expected to fully optimize the flow. Indeed, significant improvements of the distribution between cavities is expected if a major morphing, that actually straightens the obstructions, is applied. Nevertheless, results obtained for the nasal resistance and the improving trend obtained for the flow partitioning of P2 clearly show that the optimization procedure is tending towards the correct direction.
Broadening the picture concerning the adjoint

phase, the most crucial and critical feature that is worth discussing is the definition of the most suitable cost function. Indeed, this aspect of the procedure also represents its main current limitation. Herein, the dissipated power was found to grant complete results locating all major anomalies. Nevertheless, this cost function has been thought to deal with obstructions similar to the ones previously analyzed and, also in these cases, it is not granted that it represents the best possible option. As such, a more precise alternative that models in a more complete manner patients' perception can be considered in future analysis. In particular, there may be the possibility of defining a more general cost function that correctly accounts for all the functionalities of the nose including, for example, humidification, filtration and heating of breathed air. In practical terms, there is the possibility of exploiting the linearity of the adjoint equations and defining an objective function as a sum of several contributions that consider all these aspects individually.

5. Conclusion

In the current medical practice, the scarce efficiency of septoplasties has to be ascribed to the lack of a standardized and patient-specific method that measures the main features of obstructions. To deal with this issue, an innovative CFD procedure that hinges upon the adjoint-based optimization theory has been described. The reported results proved how this tool is able to locate all deviations and, at the same time, to provide quantitative information that ENT specialists can use when they are defining the most suitable approach to follow during surgeries.
As a matter of fact, even though valuable outcomes were obtained, further research is needed before making this CFD method an actual clinical tool. In particular two main aspects can be considered for future studies: (1) the definition of a new cost function of more general validity and (2) the evaluation of the robustness of the results when the expiration phase is considered. Nevertheless, this work represents an innovative and essential step for the application of the adjoint formulation to the CFD study of the nasal airflow and strongly lays the foundations for the introduction of a robust and patient-specific tool for the evaluation of septal deviations.

Acknowledgements

I would like to thank those who have made their contribution to the implementation of this paper. I would like to express my heartfelt thanks to Professor Quadrio for its constant support and for giving me the opportunity of exploring a field I have always been interested in. My gratitude goes also to Professor Trimarchi, Doctor Tanzini and Ing. Schillaci whose competences have been vital for the realization of this work.

References

[1] P. B. Dinis and H. Haider. Septoplasty: Long-term evaluation of results. *American Journal of Otolaryngology*, 23(2):85–90, March 2002.

[2] I. Hörschler, W. Schröder, and M. Meinke. On the assumption of steadiness of nasal cavity flow. *Biomechanics*, 43:1081–1085, 2010.

[3] Y. Liu, E. A. Matida, J. Gu, and M. R. Johnson. Numerical simulation of aerosol deposition in a 3-D human nasal cavity using RANS, RANS/EIM, and LES. *Journal of Aerosol Science*, 38(7):683–700, July 2007.

[4] C. Othmer. A continuous adjoint formulation for the computation of topological and surface sensitivities of ducted flows. *International Journal for Numerical Methods in Fluids*, 58(8):861–877, November 2008.

POLITECNICO
MILANO 1863

SCUOLA DI INGEGNERIA INDUSTRIALE
E DELL'INFORMAZIONE

Fluid dynamics optimization for the surgical treatment of septal deviations

Tesi di Laurea Magistrale in
Aeronautical Engineering - Ingegneria Aeronautica

Marcello Macellari, 941214

Advisor:
Prof. Maurizio Quadrio

Co-advisors:
Prof. Matteo Trimarchi
Ing. Andrea Schillaci
Dott. Umberto Tanzini

Academic year:
2020-2021

Abstract: Nasal septal deviations commonly cause obstructions of the nasal airways; when severe, deviations are surgically corrected by ear-nose-throat (ENT) specialists. Septoplasty, however, has a low success rate when the actual post-surgical benefits are considered, owing to a lack of standardized clinical tools capable to properly assess type and severity of obstructions, which vary wildly in shape and location. Often fully restoring the septal wall is impossible, and sometimes it is not required. This paper introduces a procedure, based on patient-specific Computational Fluid Dynamics (CFD) simulations, to support ENT surgeons in septoplasty planning. The method hinges upon the adjoint-based optimization theory; by minimizing a cost function that indirectly accounts for viscous losses, a sensitivity map is computed on the mucosal wall which shows if and how much the removal of each point would contribute to easing the obstruction. The optimization is applied to three real nasal anatomies reconstructed from CT images of patients affected by complex septal deviations. The sensitivity map is consistently found to identify all the anomalies correctly; the surgical action suggested by the sensitivity map appears to be feasible. Improvements in the characteristics of the nasal airflow after optimization were proved performing a suitable morphing of the geometries.

Key-words: septal deviations, septoplasty, CFD, adjoint formulation, patient-specific procedure

1. Introduction

Nasal Airway Obstructions (NAO) are one of the main medical conditions for which patients consult ear-nose-throat (ENT) surgeons [2]. Indeed, more than a third of the world's population present these symptoms [17] [15] which imply a reduction of the total amount of air passing through the nose determining relevant impacts on the quality of life [27] [34]. Among the main anatomical aetiologies causing NAO, septal deviations have been found to be the most common ones with a prevalence of 76% [5]. In these circumstances, to restore a correct respiration and relieve the discomfort of patients, ENT specialists are required to perform septoplasty operations. Nevertheless, even though only in the 3% of cases these surgeries present severe complications [6], when the actual post-surgical benefits are considered, the success rate of septoplasty falls below 80% [33] [32] resulting in a relevant social and financial burden for the entire healthcare system.

The main reason behind this inefficiency has to be found in the lack of standardized and precise clinical tools that properly evaluate the type and the severity of obstructions providing surgeons with information they can use in the definition of the most appropriate surgical approach [7] [28].
In this context, Computational Fluid Dynamics (CFD) has become a valuable tool to investigate the behavior of the nasal airflow, measure its characteristics and relate them with the local anatomy [16]. For instance, [3], [18], and [14] used CFD to evaluate the main changes in the respiratory pattern when septal deviations of different severity and typology occur. [20] and [25], instead, performed simulations of the nasal airflow to analyze which quantities, among those measured with existing clinical tools, are the most representative of the perception of patients. Furthermore, several studies have directly examined the effects of septoplasties. Among all of them, the works by Campbell et al. [1] and by Ramanthan et al. [26] are worth mentioning. The former focuses on anterior septoplasty and analyzes the nasal airflow of ten healthy subjects in order to understand the relation between the widening of the region with minimal cross-sectional area and the actual benefits of surgeries. Ramanthan et al., instead, based on the CFD results obtained on twelve pre- and post-operative CT data, suggest that the main regions of obstruction can be identified evaluating areas of maximum pressure, velocity and shear stress distribution. As a matter of fact, even though extremely valuable, all these works still rely on the subjective interpretation of CFD results thus not providing standardized and reproducible information.
The main goal of this work is to lay the foundation for the development of a reliable and robust procedure that is able to grant patient-specific and precise data on the characteristics of major deviations and obstruction in order to help ENT surgeons during the diagnostic process and in septoplasty planning. The main idea behind this method is the inclusion, in the usual CFD study of the nasal airflow, of the adjoint-based theory that is used to compute sensitivity derivatives for a shape optimization problem. The procedure simulates the airflow within nasal cavities and subsequently uses the adjoint equations to compute sensitivity values for the entire nasal surface. The final sensitivity map shows if and to what extent the displacement of each point of the surface, which would correspond to a surgical removal, is favorable or counterproductive in terms of minimization of a cost function that models the resistance to the passage of air. The method is applied to three nasal anatomies of patients affected by complex septal deviations and its validity is proved showing the final results to ENT surgeons who analyze the feasibility of suggested displacements. Furthermore, corrections identified by the procedure are virtually performed, with a suitable morphing of the reconstructed geometry, to verify improvements in terms of flow partitioning and nasal resistance.
This work has been developed starting from the conclusion derived by [29] that have been further expanded and deepened considering a wider variety of patients and refining some steps of the procedure.

2. Adjoint-based optimization

Central and most crucial step of the entire procedure is the application of the adjoint technique for the computation of the surface sensitivity values for a shape optimization problem. Therefore it is worth introducing the main theoretical and technical aspects behind the adjoint formulation used in this work. Nevertheless, it has to be remarked that all conclusions on the adjoint method presented hereafter are generally applicable for dealing with surface optimization and are not directly referred to the peculiar case under analysis. Indeed, the way this technique was specialized for the study of the nasal airflow is explained in the following section where the entire methodology behind the proposed CFD tool procedure is introduced.
In general, shape optimization problems aim at finding the optimal shape of an object that minimizes a certain cost function while complying with given constraints. When applied to CFD-based procedures, they can be written in the form:

$$\begin{aligned} &\text{minimize } f = f(\mathbf{U}, \beta) \\ &\text{subject to } R(\mathbf{U}, \beta) = 0 \end{aligned} \tag{1}$$

where f is the cost function to minimize, $\mathbf{U}$ the collection of fluid dynamic variables, β the one of control variables and R the set of constraints that is given by the Navier-Stokes equations. According to this setting, the sensitivity derivatives, namely the gradients of the cost function with respect to the control variables, give information on the influence that changes in β have on f. If β is specified as the set of displacements of all solid boundary points in the direction normal to the surface, then the so-called surface sensitivity map can be computed. When specialized for the study of the nasal cavities this aspect corresponds to the evaluation of the contribution of the removal of each point to easing the obstructions.
Within this context, the adjoint formulation can be introduced for the actual computation of the sensitivity derivatives in those cases where a high number of control variables is involved. Indeed the adjoint methodology obtains all values of sensitivity by solving two systems of two Partial Differential Equations (PDEs) thus requiring a computational time that is almost independent with respect to the number of elements of β. The first set

of equations are the governing equations of fluid dynamics whereas the second one comprehends the so-called adjoint equations that are derived starting from the Navier-Stokes ones. If other analytical methods such as direct differentiation and finite differences were to be considered they would have resulted in an unmanageable computational cost as elements of β increased in number.
In practice two different approaches can be followed for dealing with the adjoint formulation and deriving the two adjoint PDEs: the discrete one, known as "discretize then derive" and the continuous one, described as "derive then discretize". Herein, the adjoint continuous formulation specialized for ducted flows and derived by Othmer [22], has been used as the starting point for the main analytical derivations. In this regard, it should be noted that all results presented hereafter have been obtained considering a cost function with contributions exclusively on the boundaries Γ of the geometry being a common characteristic of shape optimization problems.
First of all, following the general mathematical approach for the adjoint methodology, in order to account for the set of constraints R, the optimization problem was reformulated using the method of the Lagrange multipliers. To this extent, to define the associated Lagrangian function (L), a number of Lagrange multipliers equal to the number of constraints had to be introduced. These four Lagrange multipliers are the so-called adjoint variables: the adjoint pressure q and the adjoint velocity $\mathbf{v}$ with its three components. These quantities have exactly the same units of measure of their flow variables counterparts p and $\mathbf{u}$ but they have a completely different physical meaning. The resulting Lagrangian function, that was defined over the entire domain Ω reads:

$$L = f + \int (\mathbf{v}, q) R d\Omega \tag{2}$$

With the definition of L the needed sensitivities were computed starting from its total variation that was written as:

$$\delta L = \delta_\beta L + \delta_{\mathbf{u}} L + \delta_p L \tag{3}$$

At this point, the adjoint variables, that can have arbitrary values, were chosen such that the sum of the variations of L with respect to the state variables was equal to zero:

$$\delta_{\mathbf{u}} L + \delta_p L = 0 \tag{4}$$

Then, the influence of β on the Navier-Stokes equations, i.e. the constraints of the problem, was evaluated. Indeed, the previous equality leaves $\delta_\beta L$ as the only contribution to the variation of the Lagrangian function. The final expression for the sensitivities was obtained following the approach proposed by [31] and reads:

$$\frac{\partial f}{\partial \beta_i} \propto \mathbf{v}^i \cdot \mathbf{u}^i \tag{5}$$

where β_i is the displacement normal to the surface of cell i and $\mathbf{u}$ is the velocity field of the fluid. Consequently, to compute all sensitivities there is the need of evaluating $\mathbf{v}$ and $\mathbf{u}$ over the entire domain and thus solving the previously mentioned systems of PDEs.
If the flow governing equations are known, the adjoint equations that govern the variations of both the adjoint quantities $\mathbf{v}$ and q can be derived starting from Equation 4 and computing the needed analytical derivatives. For the formulation herein reported, the resulting adjoint equations were written as:

$$\nabla \cdot \mathbf{v} = 0 \tag{6}$$

$$-\nabla \mathbf{v} \cdot \mathbf{u} - (\mathbf{u} \cdot \nabla)\mathbf{v} = -\nabla q + \nabla \cdot (2\nu \mathbf{D}(\mathbf{u})) \tag{7}$$

where $2\mathbf{D}(\mathbf{u}) = (\nabla \mathbf{u} + (\nabla \mathbf{u})^T)$.
Reminding that the selected cost function has contributions exclusively on the boundaries of the domain it can be noted that both equations do not depend on its specific shape thus giving them a general validity that holds for any adjoint-based optimization process with these characteristics.
All mathematical details for this derivation can be found in the work by Othmer and are not reported here for sake of clarity. Nevertheless it is worth mentioning a relevant hypothesis that has been crucial for deriving the adjoint equations, that is the one of *frozen turbulence*. This hypothesis assumes that variations of all turbulent quantities with respect to the project variables are negligible thus resulting in the possibility of avoiding the derivation of the adjoint counterparts of the turbulence model equations if RANS approach is used to compute the flow variables. In practical terms, *frozen turbulence* allows the reduction of the computational costs without influencing the overall behavior of the sensitivity map [30]. Regarding the adjoint equations, it has to be noted that the unknowns are only the adjoint variables. The flow variables, that in the context of the adjoint methodology are called direct or primal variables, are known and they are the ones obtained at the end of the previous simulation, called direct simulation, which solves the system of the governing equations.

Nevertheless, in order to solve the differential system of Equations 6-7, boundary conditions have to be specified. Their expressions can be obtained considering the contributions on the boundary Γ that are present in Equation 4 when the derivatives of the cost function are explicitly computed. However, their definition depends directly on the derivatives of the part of the cost function defined on the boundary and a general form, independent of the exact shape f, can not be determined.
Considering these aspects of the adjoint formulation it is now possible to introduce the exact method behind the proposed CFD procedure along with the peculiar cost function selected for this work and the resulting adjoint boundary conditions.

3. Methods

In order to apply the adjoint formulation to the computation of the surface sensitivity values of nasal walls some preliminary steps, starting from the three-dimensional reconstruction of CT scans, are needed.
For this study, a total of three CT images were chosen from a pool of available scans. These images were selected by surgeons since they present septal deviations for which the most appropriate surgical approach is not immediately identifiable with available clinical tools.
P1, a 44-year-old male, presents a complex septal deviation. The major components are a left deviation of the quadrangular cartilage and a posterior, lesser deviation of the vomer bone. It also presents a slight right deviation of the antero-superior portion of the nasal septum, at the articulation between the quadrangular cartilage and the perpendicular plate of the ethmoid bone. P2, a 30-year-old male, has the anterior portion of the quadrangular cartilage that is deviated towards the left nasal fossa, partially occluding it. Posteriorly, it presents an important right bone spur, bridging the middle meatus. Further posteriorly, it shows another left bone spur, reaching the posterior portion of the middle turbinate. P3, a 40 year-old-male, presents a nasal valve collapse (more evident in the left nostril) and a left septal deviation. The deviation involves the quadrangular cartilage, which is dislocated laterally and reaches the left inferior turbinate. Posteriorly it presents a left condro-vomerian spur that reaches the middle meatus. There is also a minor bony spur in the right posterior nasal fossa. In this case, the patient probably underwent turbinoplasty before the CT scan, as the inferior turbinate mucosa is much less hypertrophic than normally expected.
Figure 1 shows two coronal slices for each patient visualized in correspondence of critical deviations. On top, the anomalies in the anterior part of the nasal cavities are presented. Below, for each patient, one of the septal deviations in the posterior region can be observed. Images are rendered with the application of a white filter that highlights the presence of air.

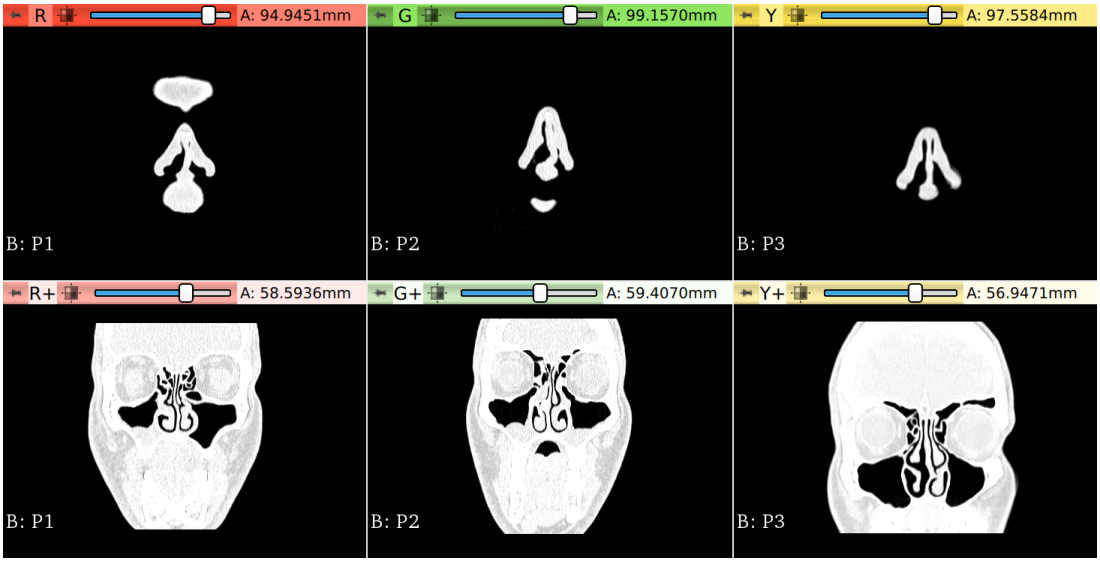

Figure 1: Coronal sections of the three patients visualized in correspondence of major deviations. On top, the deviations of the quadrangular cartilage are shown for P1 and P2 whereas the nasal valve collapse is reported for P3. Below, the left deviation of the vomer bone, the posterior part of the right bone spur and the left condro-vomerian spur are reported respectively for P1, P2 and P3

All images were provided by San Raffaele Hospital and have an acquisition matrix of 512x512 pixels. CT scans of P1, P2 and P3 have, respectively, a spatial resolution in the sagittal-coronal plane of $0.39mm \times 0.39mm$, $0.31mm \times 0.31mm$ and $0.46mm \times 0.46mm$ and a gap between consecutive axial slices of $0.925mm$, $0.925mm$

and $0.4mm$.
All CT scans were visualized and elaborated with the free and open-source software 3D Slicer [8]. The three-dimensional reconstruction of the boundaries of the nasal airways was obtained through the image segmentation process of the *Segment Editor* module [23] applying a segmentation threshold of -475HU, in accordance with the results by [21] and by [38]. Furthermore, given the major influence of the selected threshold on the final outcome, its value was verified following the approach proposed by [35] who computed it as the average of the radiodensity values of clean air, -1000HU, and of the surrounding soft tissues. In the case of nasal airways, these tissues are the nasal mucosa whose radiodensity value varies between 0HU and 50HU [10] thus confirming -475HU.
To ensure high quality results, the reconstructed geometries were refined using the options *smoothing* and *decimate* of 3D Slicer. As for the former, a sinc filter with a degree of the approximated polynomial of 0.16 was used. As for the latter, the associated parameter was set to 0, despite the default value of 0.1, in order to preserve high accuracy. At this point, the reconstructed models were extracted and saved in STereoLithography (STL) format.
Figure 2 shows the final STL file for P2. Nasal airways up to the initial part of the nasopharynx, including all paranasal sinuses, are clearly visible.

Figure 2: Final three-dimensional geometry obtained at the end of the segmentation process for P2

Then, the reconstructed geometries were used as inputs for the creation of the computational meshes. To this extent, `snappyHexMesh`, a tool contained in the open-source CFD package OpenFOAM, was adopted. In this process, an additional STL file was created to simulate the external environment. This was a small sphere, with a diameter of $70mm$, that was properly cut so as not to obstruct the internal nose. This geometry was chosen since it is thought to be a good balance between the increase in the number of cells and the possibility of ensuring an inlet flow without preferential directional information.
Figure 3 shows the mesh obtained at the end of this procedure for P2.

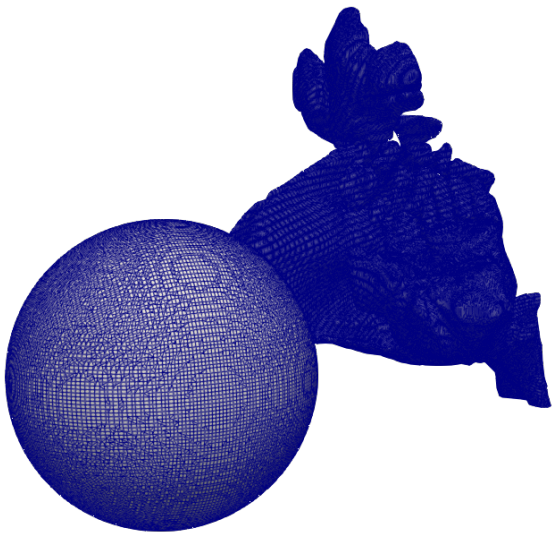

Figure 3: Final computational mesh obtained for P2

Finer cells can be observed in correspondence of the nasal airways and of the paranasal sinuses whereas a coarser grid is used for the inlet sphere. This choice kept the number of cells under control without compromising the quality of the results where the surface sensitivity is computed. Furthermore, it has to be noted that no layers were added in any of these regions. Table 1 reports the number of cells for the entire mesh and for the boundary of the nasal airways alone for the three patients. In all cases more than 5 million elements have been obtained for the inner mesh whereas around 1 million cells characterize the solid boundaries, i.e. the nasal walls. As a matter of fact, these features of the computational grids confirm the possibility of having valid and precise results without requiring excessive computing resources. Even though the same refinement was used, a different number of elements has been obtained for the three patients due to the different dimensions of the anatomies.

	Number of cells	
	Total Mesh	Solid Boundary
P1	5262788	950327
P2	5695738	1052087
P3	6623922	1178278

Table 1: Characteristics of the meshes for the three patients under analysis

Following the generation of the computational mesh, the next step was the execution of the flow solver to compute the flow variables needed for the adjoint procedure. Indeed, referring to the characteristics of the adjoint optimization previously introduced, this phase corresponds to the solution of the first system of PDEs. The solver `simpleFoam`, available in OpenFOAM, was used to perform a stationary, incompressible and turbulent simulation with a given constant flow rate of $15l/min$, which corresponds to a breathing rate at rest. All modeling choices were defined based on relevant works found in literature who proved their accuracy for the peculiar flow rate that was considered [12] [19]. Since mass transfer and heat contributions were not treated, the Reynolds-Averaged Navier-Stokes (RANS) equations were used to guarantee the conservation of mass and momentum. These equations are obtained by averaging in time the Navier-Stokes equations and read:

$$\nabla \cdot \overline{\mathbf{u}} = 0 \tag{8}$$

$$\nabla \cdot (\overline{\mathbf{u}}\,\overline{\mathbf{u}}) + \nabla \cdot (\overline{\mathbf{u}'\mathbf{u}'}) = -\frac{1}{\rho}\nabla \overline{p} + \nu \nabla^2 \overline{\mathbf{u}} \tag{9}$$

where $\overline{p}$ represents the mean pressure field, $\overline{\mathbf{u}}$ the mean velocity field and $\mathbf{u}'$ its fluctuating component. To solve this system of equations an appropriate turbulence model was introduced. In this work, the Menter's Shear Stress Transport or k-ω SST RANS model was chosen for two main reasons: (1) its ability of providing good and numerically stable results both in the near-wall region and in the far field region and (2) its prevalence in the CFD studies of the nasal airflow [13]. In performing the simulations, the default standard values of the coefficients of this turbulent model were used.
At this point, boundary conditions were specified. At the inlet, the value of the mean velocity was assigned to result in a net flow rate equal to the value previously defined. The no-slip and no-penetration conditions, i.e. $\overline{\mathbf{u}}$=0, were applied on the boundaries of the reconstructed geometry whereas, at the outlet, located in the nasopharynx, the zero gradient condition was applied. For the mean pressure the zero gradient was applied at the inlet and on the boundaries of the nasal cavities whereas at the outlet a reference value was specified. Regarding the turbulent quantities, wall functions were used to reduce the number of grid points needed at the wall.

3.1. Computation of surface sensitivity map

Final phase of the process is the computation of the surface sensitivity map. As such, to specialize the general adjoint method previously introduced the most suitable cost function was selected.
Considering the aim of the procedure, the dissipated power was chosen as the quantity to be minimized. Indeed, it is thought to represent the resistance that the nasal airflow encounters and that increases when obstructions are present. In particular, dissipated power was not written directly in terms of viscous losses but as the integral across the boundary of the net mechanical energy flux, computed as the sum of the flow energy (p=P/ρ) and the kinetic energy that represents momentum losses. In point of fact, this quantity is equal to the viscous losses

but yields an easier expression to handle written as:

$$f = \int_{\Gamma} d\Gamma (p + \frac{1}{2}u^2)\mathbf{u} \cdot \mathbf{n} \tag{10}$$

where Γ represents, in this case, the mucosal walls. Furthermore f depends only on the flow variables. In this regard, it has to be noted that even though the cost function does not depend on β these quantities still have an influence on R.
With the definition of f also boundary conditions were specified. At the inlet and at the solid walls the same conditions of p and $\mathbf{u}$ were applied respectively for q and $\mathbf{v}$. At the outlet, instead, the boundary conditions that were derived are given by the expressions:

$$q = \mathbf{v} \cdot \mathbf{u} + v_n u_n + \nu(\mathbf{n} \cdot \nabla)v_n - \frac{1}{2}u^2 - u_n^2 \tag{11}$$

$$0 = u_n(\mathbf{v}_t - \mathbf{u}_t) + \nu(\mathbf{n} \cdot \nabla)v_t \tag{12}$$

where the subscripts t and n refer to the normal and tangential components. Since the primal variables are known and since the frozen turbulence hypothesis was used no other boundary conditions were specified. Figure 4 summarizes, with a schematic representation of the computational domain, all boundary conditions specified for the primal and the adjoint variables. This emphasizes once more the major advantages of using the adjoint formulation: all sensitivities are computed at the same time with the solution of two systems of PDEs with their own boundary conditions specified on the same domain and computational grid.

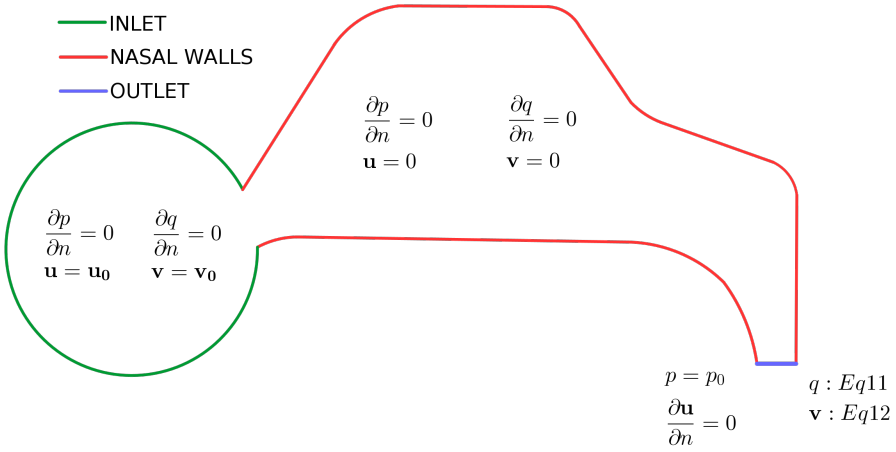

Figure 4: Schematic representation of the computational domain with the primal and adjoint boundary conditions for inlet, nasal walls (i.e. solid boundary) and outlet

In practice, to solve the adjoint equations and compute the surface sensitivity values, a solver implemented in OpenFOAM was used. This solver uses the `simpleFoam` algorithm to solve for the adjoint variables and subsequently uses the adjoint velocity field to calculate the surface sensitivity map. With respect to its original form the solver was modified to adapt to the version 7 of OpenFOAM and to account for laminar simulations. The outputs from this solver include the value of the cost function, the adjoint flow fields and the normalized sensitivity values.

4. Results

All results were found to be independent with respect to the adopted spatial discretization. In particular, grid independence was verified from a qualitative point of view for all patients focusing on the behavior of the sensitivity map. Furthermore, considering the results shown hereafter, it is important to notice that they are described adopting the point of view of the patients: the left nasal cavity is the one on the left of the patient and the same holds for the right one.

4.1. RANS

First, an overview of the results obtained for the flow variables at the end of the direct simulation is provided. This is done to highlight the major effects of septal deviations on the characteristics of the nasal airflow. In particular, values of $\mathbf{u}$ and p are visualized for P2 since he is the one that presents the most critical anomalies.

Figure 5 shows two three-dimensional views of the velocity flow field, pictured in terms of its streamlines. Concerning the features directly related to anatomical anomalies, an important recirculating region can be observed immediately after the left deviation of the quadrangular cartilage. Here the magnitude of the velocity is around $1m/s$ and this value represents its minimum in both nasal fassae. Second noticeable effect of deviations is the acceleration undergone by the flow in the restriction of the inferior right meatus. Here the pick of the velocity magnitude, equal to $13.15m/s$, is reached. Overall, obstructions result in a strong asymmetry between the two nasal cavities that becomes evident computing the distribution of the volumetric flow rate. Values equal to $9.33l/min$ and $5.67l/min$ are obtained for the left and the right cavity respectively and they correspond to a percentage distribution of 62.18% and 37.82%. Always referring to the same Figure, it is worth mentioning the non-trivial acceleration that the flow undergoes near the nose tips passing from $0.32m/s$ in the external environment to more than $2m/s$. Indeed, even though not related to any deviation, this characteristic will be relevant to explain the adjoint results in this region.

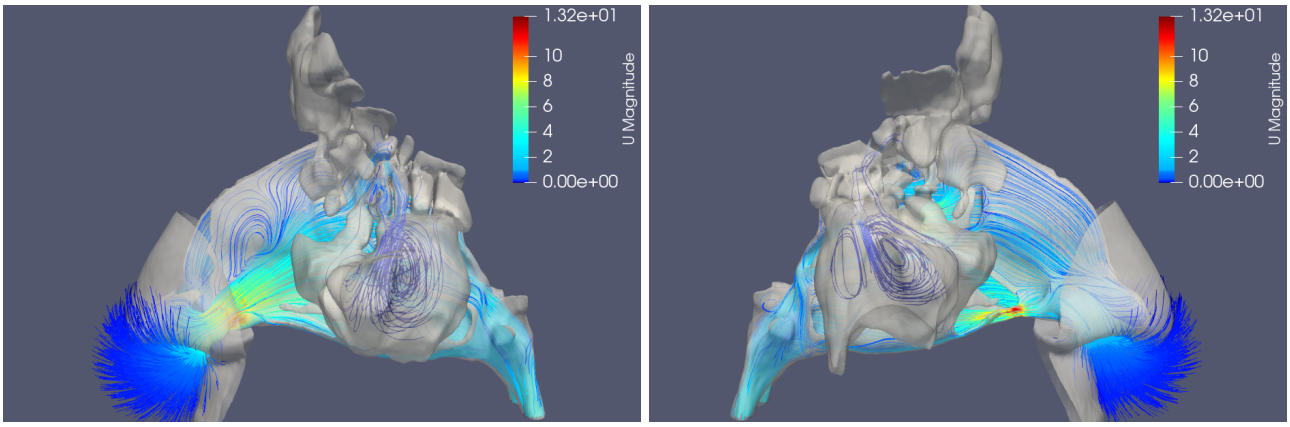

Figure 5: Streamlines of the left and right nasal cavity flow colored by the magnitude of the local velocity field for P2

Figure 6 shows the asymmetry between the two cavities in terms of pressure behavior plotted from the nasal tip down to the nasal choana. The reported values were computed at twelve different locations considering the average of the pressure field over the entire local cross-sectional area. In both cavities relevant pressure drops are present in correspondence of the obstructions. For the left nasal fossa, it can be observed that the anterior deviation causes a variation from $70m^2/s^2$ to about $22m^2/s^2$ but, after that anomaly, pressure decreases smoothly. In the right fossa, instead, relevant changes can be observed in correspondence of both points where the bone spur reaches the turbinates. In actual fact at these locations local pressure drops are even more severe than what can be noted in the Figure but since these variations interest first the inferior meatus and only after the middle one the averaging process makes them less evident.

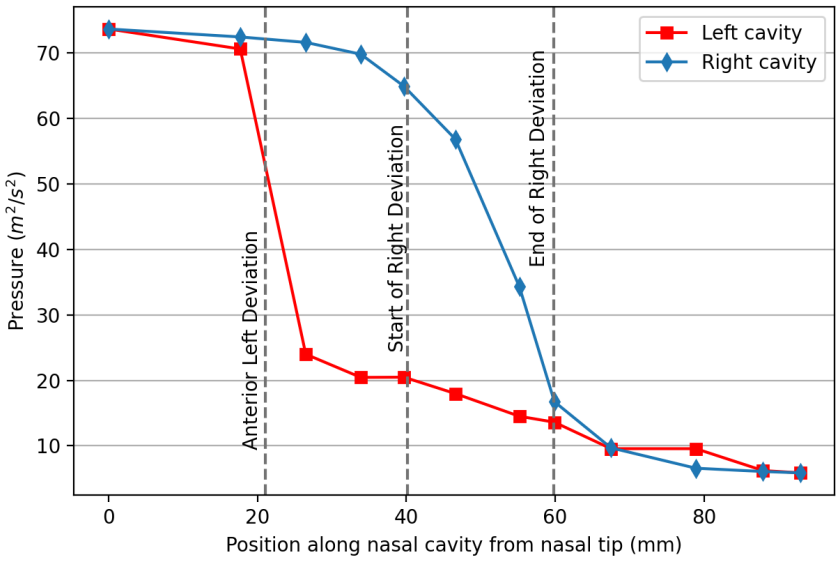

Figure 6: Pressure trend through the right and left nasal passage from nasal tip to nasal choana for P2

Table 2 reports, for all three patients, values of flow partitioning and nasal resistance that are considered two of the most meaningful quantities for the assessment of nasal obstructions. Nasal resistance was computed according to the formula proposed by [9] as $R_{nose}=\triangle p/Q$, where Q is the volumetric flow rate expressed in ml/s and $\triangle p$ is the pressure drop from nostrils to nasopharynx measured in Pa.

	Flow partitioning		
	Left cavity	Right cavity	Resistance
	%	%	$Pa/(ml/s)$
P1	32.49%	67.51%	0.091
P2	62.18%	37.82%	0.360
P3	22.93%	77.07%	0.037

Table 2: Flow partitioning and nasal resistance computed for the three anatomies

4.2. Surface sensitivity

Having presented the intermediate results for the primal variables it is now possible to focus on the surface sensitivity maps. In the following, they are shown for all three patients focusing on those regions that have been identified as the most critical ones. In particular, they are visualized in terms of normalized surface sensitivity, i.e. dividing the surface sensitivity value of each cell by the maximum value obtained over the entire domain. These results are rendered on a red scale such that the higher the intensity of the color the more critical that cell is for the minimization of the cost function. Furthermore, considering that, after normalization, high picks in the value of the surface sensitivity may tend to overshadow less critical zones, all values above 0.01 have been considered meaningful and are now reported. In practical terms, the main advantage of referring to the normalized values is that they directly provide quantitative information. Indeed they can also be interpreted as the percentage value of the local normal displacement with respect to the maximum one allowed over the entire geometry.
In order to understand the results from a surgical point of view it has to be remembered that regions with high sensitivity, i.e. those in red, would favor the minimization of the cost function with a displacement of the surface in the outwards direction with respect to the fluid volume. This would correspond to a surgical removal that widens the space where air can pass. Regions in gray, instead, are the ones that the surgeon should not touch since they would not bring actual benefit to the patients.

4.2.1 P1

Results obtained with the adjoint formulation for P1 are shown in Figure 7, Figure 8 and Figure 9. In this case, the solver has identified three main critical areas: (1) a region in correspondence of the deviation of the quadrangular cartilage, (2) one behind the right nostril and (3) one located along the left nasal fossa where there is the deviation of the septum.
Figure 7 shows, on top, a left lateral view of the nasal geometry that locates the first of these three regions and, below, a zoomed-in view that highlights its characteristics.

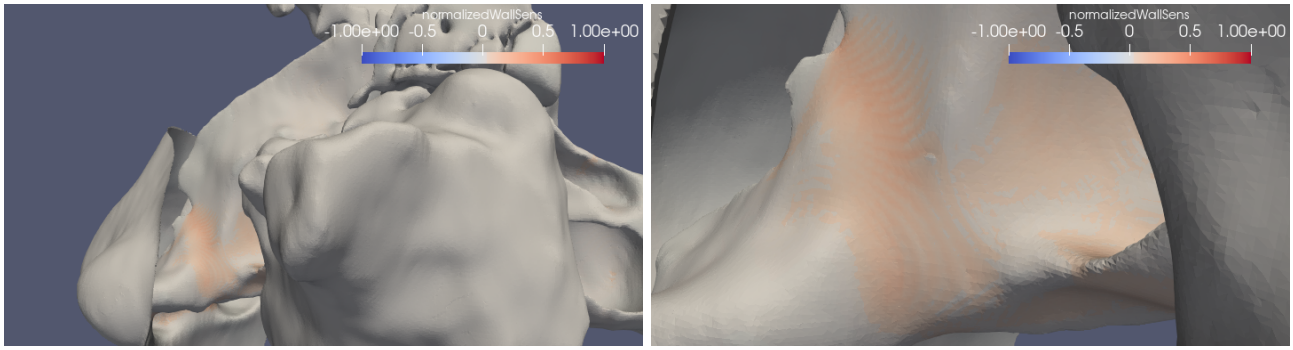

Figure 7: Surface sensitivity map for P1. On top, lateral view of the left side of the patient. Below, zoom on the region detected by the adjoint procedure

Local maxima for sensitivity are obtained in correspondence of the obstruction, i. e. in the top part of the red region, where cells have normalized values around 0.2. Nevertheless, non negligible values above 0.1, are also obtained for the lateral mucosal walls. In this sense, it has to be noted that, even though not reported in the Figure, a similar red region is computed also for the part of the nasal fossa towards the septum. Overall, these results show that the adjoint procedure would require to operate, not only on the deviation, but also on the entire cross-sectional area.
To analyze the second critical region, Figure 8 gives a global view from below on the area behind the right nostril.

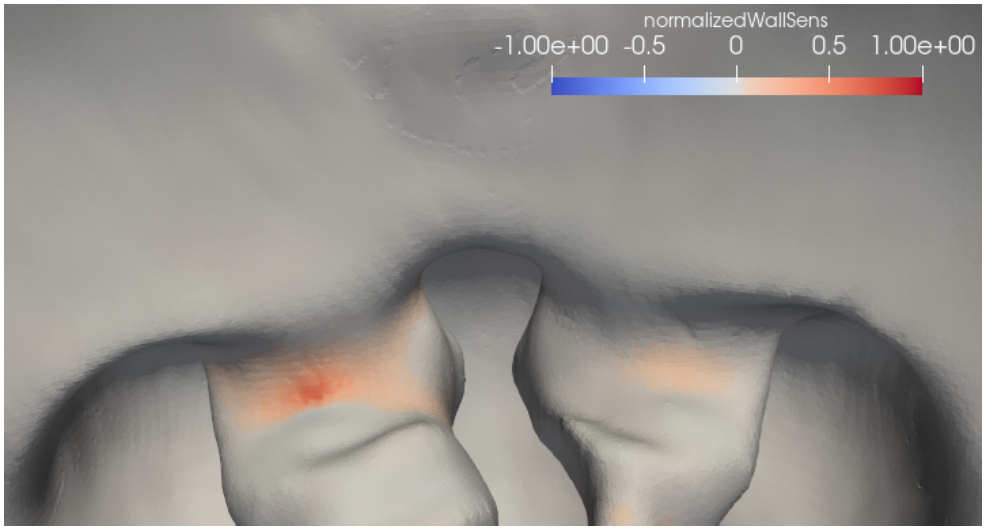

Figure 8: Surface sensitivity map for P1. View from below focused on the anterior part of the nasal airways

Here the cell with maximum sensitivity, which corresponds to a normalized result of 1, can be observed. Cells surrounding it have normalized values above 0.25 emphasizing the criticality of this region for the adjoint formulation. Close to this area, a small number of points with negative sensitivities values have been obtained. From a practical point of view, these cells would require a displacement of the surface towards the internal part of the geometry but their presence is mainly ascribable to numerical oscillations caused by sharp variations of the adjoint quantities. Nevertheless, the fact that they are not rendered in blue highlights that their values are close to zero thus confirming the validity of the results.
In conclusion, the critical area detected in correspondence of the left deviation of the vomer bone is shown in Figure 9. Here, normalized sensitivity values around 0.03 have been obtained suggesting a displacement towards the right fossa aimed at straightening the distortion. It should be noted that this deviation has been identified and evaluated even though it does not cause a severe obstruction thus proving the general validity of the procedure and of the selected cost function.

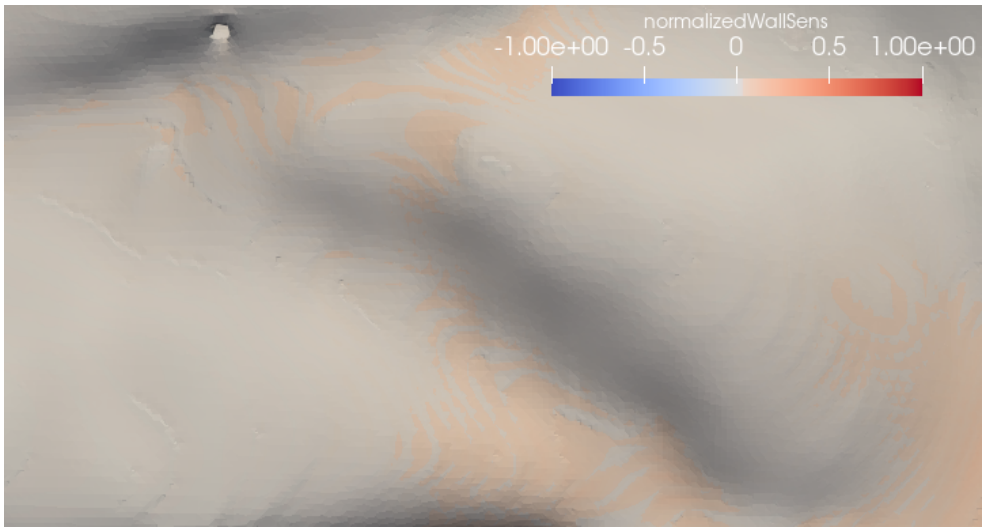

Figure 9: Surface sensitivity map for P1. View from the "inside" of the left deviation

4.2.2 P2

Adjoint results obtained for P2 are shown in Figure 10 and Figure 11. In particular, the first one focuses on the sensitivity map obtained in correspondence of the left anterior deviation. The global surgical approach that the adjoint identifies for this region is very similar to the one found for the anterior septal deviation of P1 and would suggest to operate in order to widen the entire cross-sectional area. However some differences with respect to the previous anatomy can be observed when the punctual values of sensitivities are considered. As a matter of fact, also in this case, the zoomed-in view shows that the major criticality is obtained in correspondence of the obstruction, i.e. in the top part of the red region. Nevertheless, for P2, this portion corresponds also to the global maximum. Indeed, it is in this area that it is possible to notice the unit value of the normalized sensitivity. Furthermore, Figure 10 shows that all other points around it have values above 0.35 and would significantly contribute to the optimization of the cost function. Considering the remaining cells rendered in red, the ones on the lateral walls of the cavity, they have values above 0.05 that are slightly smaller than the ones of P1 in the same position.

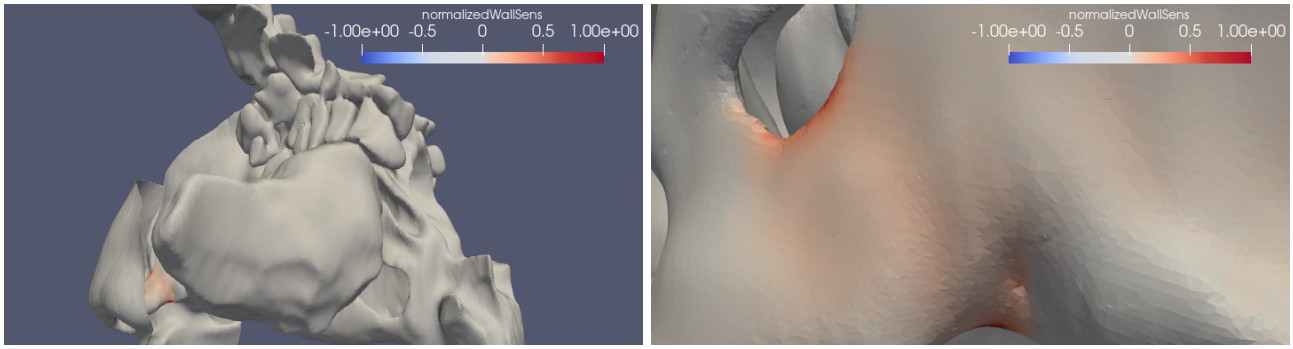

Figure 10: Surface sensitivity map for P2. On top, lateral view of the left side of the patient. Below, zoom on the details of the sensitivity map computed for the restriction

Figure 11, instead, shows a global view of the nasal cavities seen from the right side of the patient in order to emphasize two other critical regions. These areas, that are highlighted in the zoomed-in views, are located where the right bone spur touches the inferior turbinate (image on the right) and the middle one (image on the left) causing major obstructions. In both cases the adjoint procedure would suggest to widen the restriction even though higher normalized sensitivity values are obtained in correspondence of the inferior meatus. Here, an important contribution for the minimization of the cost function, can be obtained with an upward displacement of the cells on top of the restriction that have a normalized value of 0.4. Nevertheless, important improvements may be obtained also operating on the other points of this restriction where the solver computed values around 0.2. Considering the obstruction in correspondence of the middle turbinate, instead, it is possible to see that the adjoint formulation would suggest to operate in two different locations. The first one is in correspondence of the middle meatus where a restriction similar to the one just discussed is present. Here, all cells have comparable results around 0.1 and there is not a major critical point where to intervene to bring benefit to the patient. The second location, instead, is the part of the left nasal cavity in between the deviated septum and the turbinate and is characterized by normalized values around 0.04 that would suggest, also in this case, a minor operation to widen the area.

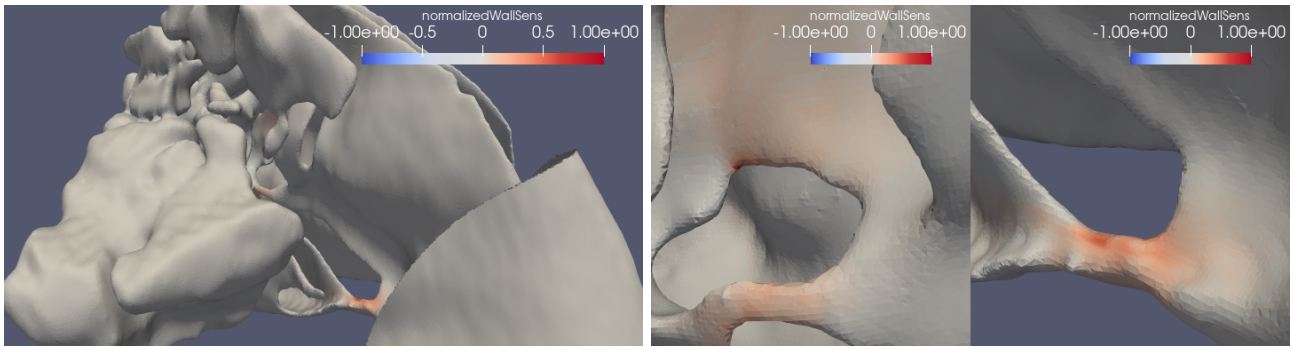

Figure 11: Surface sensitivity map for P2. On top, lateral view from the right side of the patient. Below, zoomed-in views on the two restrictions caused by the right bone spur

4.2.3 P3

To complete the presentation of all the adjoint results, Figure 12, Figure 13 and Figure 14 show the surface sensitivity map computed for P3. In this case five major regions have been identified as critical areas where surgeons should operate. These are: (1) the obstruction caused by the NVC, (2-3) the start and the end point of the contact region between the left septal deviation and the inferior turbinate, (4) the obstruction caused by the left condro-vomerian spur that reaches the middle turbinate and (5) a region behind the right nostril. Figure 12 shows the location and the characteristics of the first of these areas.

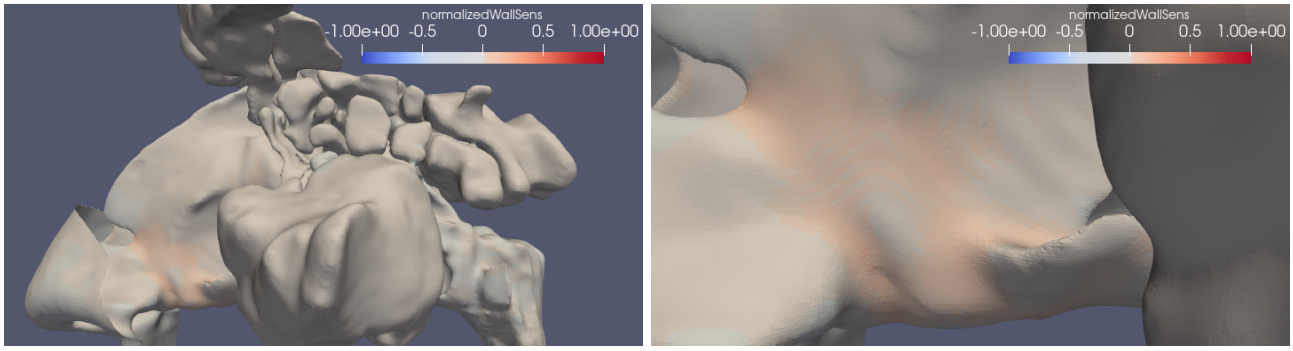

Figure 12: Surface sensitivity map for P3. On top, left lateral view. Below, zoom on the region of interest where high sensitivity values are visible

Here, the solver would suggest to operate on the entire cross-sectional area in correspondence to the collapse of the nasal valve with an outward displacement. From a quantitative point of view the highest values of sensitivity are obtained in the top and in the bottom part of the section and are equal to 0.1 whereas the other red cells are around 0.045. Also in this case a specular red region is obtained in the internal part of the nasal cavity with a percentage displacement around 0.3 as shown in Figure 13. Here a view on the left nasal cavity of P3 seen from the inside is shown. This visualization was obtained with a proper clip of the geometry and highlights also the critical regions caused by the left septal deviation. First, the starting point of obstruction with the inferior turbinate can be analyzed. Here the solver has computed values of the normalized sensitivity around 0.04 and this red region also involves a small portion of the meatus and the bottom part of the nasal cavity. In correspondence of the point that represents the end of the contact, instead, smaller values around 0.025 can be observed. Finally, it is possible to consider the obstruction caused by the left condro-vomerian spur in correspondence with the middle turbinate that is the one highlighted in the zoomed-in view. Here the adjoint procedure gives a normalized value of 0.015 and would suggest opening the passage for air.

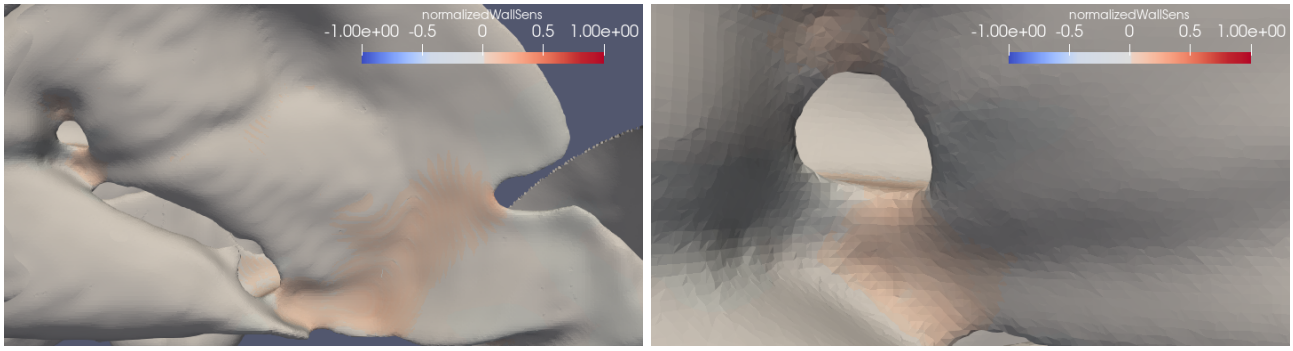

Figure 13: Surface sensitivity map for P3. On top, view of the left nasal cavity from the "inside". Below, zoom on the obstruction of the middle meatus

Figure 14, in the end, shows the critical region behind the right nostril. In this area, the adjoint formulation would require an average percentage displacement of 0.25 with some cells that have a pick of 0.35. Furthermore, as it happened for P1, in this region some points that would require a negative displacement can be observed. To conclude the analysis of P3, even though it is not shown in any Figure, it is worth mentioning that values of normalized sensitivity slightly above 0.01 have been obtained also for the minor bony spur in the right posterior nasal fossa. In particular, for this anomaly, the adjoint formulation would suggest to operate with a percentage outward displacement, aimed to straighten the deviation, around 0.011.
As a general consideration that is valid for all the reported results, it can be observed that red regions are characterized by a faint strip pattern. This is ascribable to the mesh discretization that is used. Nevertheless,

with grid convergence, it was proved that this characteristic does not influence the quantitative values of the cells in the region.

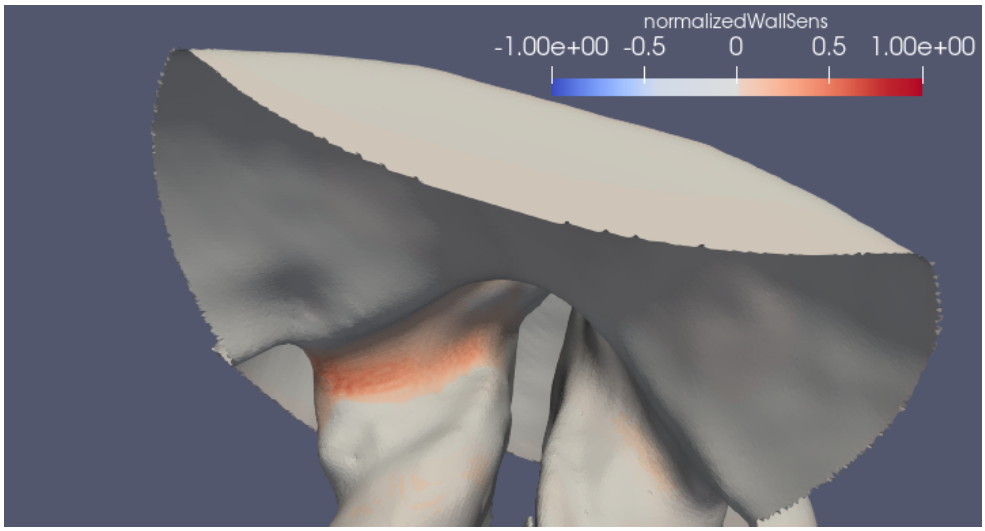

Figure 14: Surface sensitivity map for P3: view from below. A critical region detected by the adjoint formulation is shown in behind the right nostril of the patient

5. Discussion

An innovative CFD adjoint method developed to help ENT surgeons in the planning of septoplasty operations, has been described. The preliminary three steps of the procedure, namely the segmentation of CT scans, the creation of the computational mesh and the set up of the direct simulations, are usual phases of any CFD study of the nasal airflow and, herein, they were designed to result in a linear sequence of operations able to guarantee accurate results. Indeed, any adjoint simulation starts, for the computation of sensitivities, from the values obtained for the primal variables and hence is strongly influenced by their quality. Consequently, it is worth mentioning some critical conclusions that this work has highlighted also for the preliminary steps.
For all CFD studies of the nasal airflow, during the segmentation process, the choice of the radiodensity threshold is the most crucial decision. As a matter of fact, the value selected in this work, equal to -475 HU, was found to grant a correct reconstruction of the entire upper airways. This is testified by the values of the velocity magnitude computed in the paranasal sinuses, one of the most affected parts by changes in the threshold [4] that are in perfect agreement with the work by [37]. Nevertheless, it has to be remarked that, independently on the selected threshold, the ability of the segmentation process to reconstruct the nasal airways is subject to the quality of the CT scans and to the static representation that they give of a dynamic geometry. In fact, nasal anatomy may vary over time due to the nasal cycle but these changes can not be captured by a medical imaging tool that considers a single time-point. In future work, to account for these variations, the use of nasal decongestants prior to the CT scan may be a valuable solution. Indeed, they would allow to explore the range of variation of the nasal anatomies and obtain a complete picture of the characteristics of the patients [36].
Regarding the computational mesh, instead, a relevant advancement with respect to existing works has been achieved by simulating the external environment thanks to a small sphere rather than using a wider box that surrounds the patient's head. This approach grants important savings from a computational point of view and it was found to give good quality results also close to nostrils where fictitious directional information enforced by boundary conditions become critical. If expiration is simulated an increase in the diameter of the sphere can be introduced. As far as the adjoint simulations are concerned, the curvature of the surface was found to have a relevant influence on their robustness. This resulted in the need of introducing a higher coverage of cells in those regions with high curvature like the nasopharynx.
Nevertheless, the most innovative phase of the entire procedure is the application of the adjoint-based optimization theory to deal with septal deviations. According to surgeons the adjoint formulation has correctly highlighted all parts of the nasal septum that might be identified during a routine pre-operative study of the CT scans. Furthermore, after a careful examination of the results, they confirmed that the CFD analysis suggests only modifications that are feasible form a surgical point of view: the septal components are displaced inward with respect to anatomy which is exactly what the usual surgery tries to accomplish. The only exception is in P3, where the adjoint formulation would suggest an outward displacement of the nasal valve that was correctly

identified as collapsed during the analysis of the CT images. Indeed, nasal valve collapse is often a dynamic feature of the nose of the patient that becomes evident in forced inspiration but is not usually found for normal breathing. From a surgical standpoint, the general validity of the results is confirmed also by the essentially null sensitivity computed for turbinates, paranasal sinuses and the nasopharynx. Indeed, concerning turbinates, since in all three cases no hypertrophy is present, surgeons confirmed that they would not operate to reduce their volume.
In addition to these aspects that confirmed the reliability of the proposed tool, the possibility of expressing the results in terms of normalized sensitivity values allowed to have images that can be directly interpreted by surgeons. Indeed, ENT specialists confirmed that the clear advantage in surgical planning with this kind of visualization is that the most relevant parts can be easily and directly identified by looking at the 3D reconstruction, without taking into account specific physical quantities that are often unintuitive. Furthermore, with this approach, they also have an actual indication of how much they should reduce the obstruction in order to maximize the benefits for the patients. Nevertheless, in this regard, an important remark has to be made. The smaller sensitivity values that are computed for the anatomical anomalies located in correspondence of the middle and superior meatus can be ascribed also to the reduced quantity of air present in that region and not only to the fact that they may be less critical points. As such particular attention should be given to that area while analyzing the adjoint results. Conversely, a broader reasoning is needed to discuss about the red critical regions identified behind nostrils. Indeed, in this case, the CFD indications can not be directly correlated to the surgical approach. As a matter of fact, from a fluid dynamics point of view, these results of the adjoint formulation are due to the severe acceleration that air undergoes in this part of the nose and that, in the cases of P1 and P3, happens in correspondence of a prominent nasal sill. As such, this area is seen by air as if it were a protruding step that causes major deviations resulting in a favorable region for the minimization of the dissipated power. From a medical point of view, instead, the nostril opening is considered the posterior border of the external nasal valve a region whose contribution to nasal breathing has been investigated only by a few studies and whose obstruction can be caused by many underlying problems of different nature [11]. Therefore, more than in other regions the adjoint results should be carefully evaluated.
Table 3 proves the validity of the procedure by showing the flow partitioning and the nasal resistance computed for the three anatomies after applying a suitable morphing of the geometries. In particular, all points of the nasal walls were displaced by a quantity equal to the normalized sensitivity values multiplied by $1mm$. This maximum displacement was chosen to guarantee a good balance between the possibility of measuring an improvement and the need of controlling the quality of the final STL file generated with the morphing.

	Flow partitioning						
	Left cavity %		Right cavity %		Nasal Resistance $Pa/(ml/s)$		Avg. Displacement mm
	Pre-op	Post-op	Pre-op	Post-op	Pre-op	Post-op	
P1	32.49%	32.25%	67.51%	67.75%	0.091	0.081	0.03056
P2	62.18%	60.63%	37.82%	39.37%	0.360	0.311	0.03865
P3	22.93%	23.52%	77.07%	76.48%	0.037	0.033	0.04065

Table 3: Comparison of flow partitioning and nasal resistance for the three analyzed patients computed before and after a suitable morphing of the geometries

In terms of nasal resistance relevant improvements with respect to Table 1 can be observed for all cases. Furthermore, since the inlet flow rate was not changed these variations are exclusively due to a reduction of the pressure difference between the nostrils and the nasopharynx. Concerning flow partitioning, a rebalancing of the quantity of air passing through the two nasal fossae is accomplished for P2 and P3 whereas a minor worsening, smaller than 0.3%, is computed for P1. In this regard, it should be noted that the presented procedure, with the set up previously explained, is not designed to directly solve this kind of optimization. Furthermore setting to 1mm the maximum movement applied to the geometry the resulting average displacement over all critical regions previously illustrated is quite small, below $0.05mm$ for all patients. Therefore, significant improvements of this quantity are expected with the application of a major morphing that actually straightens the obstructions. Nevertheless, results obtained for the nasal resistance and the improving trend computed for the flow partitioning of P2 clearly show that the optimization procedure is tending towards the correct direction.
Broadening the picture concerning the adjoint phase, one of the most critical and crucial aspects that should be addressed, is the proper choice of the cost function. In this work, the use of the dissipated power was found

to grant valuable and complete results with the identification and the characterization of all major anomalies reported by surgeons. However, this peculiar cost function was thought and developed to deal with obstructive problems similar to the ones previously analyzed and also in this case it should be verified if it is the best possible option. As a consequence, more precise and comprehensive alternatives that model also other functionalities of the nasal airways can be considered in future analyses. Indeed the physiology of the nose is quite complex and accounts for several needs that should be equally evaluated when trying to optimize its shape. In this regard, there would also be the possibility of exploiting the linearity of the adjoint equations and defining a more general cost function written as the sum of several contributions that represent the different feelings and needs of the patients. In practice, this process may also require the redefinition of both the direct and the adjoint equations to account for further phenomena such as heat contribution and humidification mechanisms.
Separate discussion should be made concerning the influence of the selected turbulence model on the outcomes of the procedure. In this work, the results of the entire process were found to be robust with respect to the peculiar model that is implemented. Indeed, for P3, simulations were set up using also the k-ϵ and the v^2-f RANS model in addition to the k-ω SST. Results were compared in terms of normalized sensitivity values and a variation smaller than 1% was obtained for all cells of the domain. When considering this modeling aspect it should be reminded that every turbulence model is characterized by the presence of free constants that should be properly tuned to obtain better results on a particular problem. However, in the context of nasal airflow, almost no reference exists concerning the way these constants should be set [24]. In this regard, it would be desirable to have more experimental data in order to compare CFD results with them. Nevertheless, it should be remarked that no significant effects on the final outcomes were found either when performing a laminar simulation. In this case, all quantities were noticed to differ by less than 2%. However, this small difference is valid for the peculiar flow rate that was chosen. If higher flow rates are considered turbulence is expected to become more relevant and the possibility of adopting a tool that is robust with respect to the RANS model adopted returns to be fundamental.
In the perspective of developing a method that can actually assist surgeons in planning septoplasty, the possibility of automatizing the entire procedure and, consequently, reducing the total operator time becomes a relevant aspect. As of today, the segmentation of the CT images is the only step that needs a constant and active external intervention to control the results of the reconstruction. As such, it is the most time-consuming part when operator time is considered, and it requires 10-20 min depending on the expertise of the controller. On the other hand, the following steps of the procedure can be easily automated since their set up does not depend on the peculiar segmentation. Nevertheless, these phases are also the most demanding ones in terms of computational cost. On a conventional laptop, using parallel computing on 6 cores, it took about 10 hours to obtain the surface sensitivity map starting from the reconstructed geometry. This wall clock time was reduced up to 3/4 hours using higher computational resources.

6. Conclusion

The inefficiency of septoplasty operations in relieving patients' NAO has to be ascribed to the lack of standardized and patient-specific tools that surgeons can use to gather valuable information on septal deviations. To deal with this issue, this study has described an innovative CFD procedure that integrates the usual study of the nasal airflow with an adjoint-based optimization theory that is used to compute sensitivity derivatives for a cost function that models nasal resistance. The results of this method allow surgeons to evaluate the criticality of deviations and obtain quantitative information on where they should focus their effort. The validity of the procedure was tested applying it to three reconstructed nasal anatomies. Outcomes were visualized in terms of normalized surface sensitivity maps and they demonstrated the ability of the method to characterize all anatomical alterations. Furthermore, the surgical approach proposed by the adjoint formulation was validated by surgeons who compared it with their own operative plan and confirmed its feasibility. The robustness of the procedure with respect to the peculiar turbulence that is selected when RANS equations are solved was also proved.
Of course, there remains room for improvement before making this CFD method a clinical tool that ENT surgeons can use in their daily practice. In particular, according to the authors, two main points should be addressed in future studies: (1) the definition of a new cost function of more general validity and (2) the evaluation of the robustness of the results during expiration or when different inlet flows are considered. Therefore, the results obtained till now are not considered to be conclusive, but, to the best of the authors' knowledge, they represent a first example of the application of the adjoint formulation to the CFD study of the nasal airflow in order to provide surgeons with robust and patient-specific information on which corrections are recommended to maximize the efficiency of septoplasty operations.

References

[1] D. A. Campbell, M. G. Moghaddam, J. S. Rhee, and G. J. M. Garcia. Narrowed Posterior Nasal Airway Limits Efficacy of Anterior Septoplasty. *Facial Plastic Surgery & Aesthetic Medicine*, 23(1), 2021.

[2] R. K. Chandra, M. O. Patadia, and J. Raviv. Diagnosis of Nasal Airway Obstruction. *Otolaryngologic Clinics of North America*, 42(2):207–225, April 2009.

[3] X.B. Chen, H.P. Lee, V.F.H. Chong, and D.Y. Wang. Assessment of septal deviation effects on nasal air flow: A computational fluid dynamics model. *American Laryngological Rhinological and Otological Society*, 119:1730–1736, 2009.

[4] G. B. Cherobin, R. L. Voegels, E. M. M. S. Gebrim, and G. J. M. Garcia. Sensitivity of nasal airflow variables computed via computational fluid dynamics to the computed tomography segmentation threshold. *PLOS ONE*, 13(11):e0207178, November 2018.

[5] D. W. Clark, A. G. Del Signore, R. Raithatha, and B. A. Senior. Nasal Airway Obstruction: Prevalence and Anatomic Contributors. *Ear, Nose & Throat Journal*, 97(6):173–176, June 2018.

[6] J. Dabrowska-Bien, P. H. Skarzynski, I. Gwizdalska, K. Lazecka, and H. Skarzynski. Complications in septoplasty based on a large group of 5639 patients. *European Archives of Oto-Rhino-Laryngology*, 275(7):1789–1794, May 2018.

[7] P. B. Dinis and H. Haider. Septoplasty: Long-term evaluation of results. *American Journal of Otolaryngology*, 23(2):85–90, March 2002.

[8] A. Fedorov, R. Beichel, J. Kalpathy-Cramer, J. Finet, J.-C. Fillion-Robin, S. Pujol, C. Bauer, D. Jennings, F. Fennessy, M. Sonka, J. Buatti, S.R. Aylward, J.V. Miller, S. Pieper, and R. Kikinis. 3D Slicer as an Image Computing Platform for the Quantitative Imaging Network. *Magnetic Resonance Imaging*, page 22770690, 2012.

[9] G. J. M. Garcia, N. Bailie, D. A. Martins, and J. S. Kimbell. Atrophic rhinitis: A CFD study of air conditioning in the nasal cavity. *Journal of Applied Physiology*, 103(3):1082–1092, September 2007.

[10] S. C. Gupta, M. Singh, Alok Jain, and D. K. Walia. A comparative study of radiological and antroscopic findings in the lesions of maxillary sinus. *Indian Journal of Otolaryngology and Head and Neck Surgery*, 56(1):9–13, January 2004.

[11] G. S. Hamilton. The External Nasal Valve. *Facial Plastic Surgery Clinics of North America*, 25(2):179–194, May 2017.

[12] I. Hörschler, W. Schröder, and M. Meinke. On the assumption of steadiness of nasal cavity flow. *Biomechanics*, 43:1081–1085, 2010.

[13] M. S. Islam, G. Paul, H. X. Ong, P. M. Young, Y. T. Gu, and S. C. Saha. A Review of Respiratory Anatomical Development, Air Flow Characterization and Particle Deposition. *International Journal of Environmental Research and Public Health*, 17(2):380, January 2020.

[14] N Janović, A. Ćoćić, M. Stamenić, A. Janović, and M. Djurić. Side asymmetry in nasal resistance correlate with nasal obstruction severity in patients with septal deformities: Computational fluid dynamics study. *Clinical Otolaryngology*, n/a(n/a), 2020.

[15] M. Jessen and L. Malrn. Definition, prevalence and development of nasal obstruction. *Allergy*, 52(s40):3–6, December 1997.

[16] S.C. Leong, X.B. Chen, H.P. Lee, and D.Y. Wang. A review of the implications of computational fluid dynamic studies on nasal airflow and physiology. *J. of Rhinology*, 48:139–145, 2010.

[17] C. H. Li, A. Kaura, C. Tan, K. L. Whitcroft, T. S. Leung, and P. Andrews. Diagnosing nasal obstruction and its common causes using the nasal acoustic device: A pilot study. *Laryngoscope Investigative Otolaryngology*, 5(5):796–806, August 2020.

[18] T. Liu, D. Han, J. Wang, J. Tan, H. Zang, T. Wang, Y. Li, and S. Cui. Effects of septal deviation on the airflow characteristics: Using computational fluid dynamics models. *Acta Oto-Laryngologica*, 132(3):290–298, March 2012.

[19] Y. Liu, E. A. Matida, J. Gu, and M. R. Johnson. Numerical simulation of aerosol deposition in a 3-D human nasal cavity using RANS, RANS/EIM, and LES. *Journal of Aerosol Science*, 38(7):683–700, July 2007.

[20] J. Malik, B. M. Spector, Z. Wu, J. Markley, Songzhu Zhao, B. A. Otto, A. A. Farag, and K. Zhao. Evidence of Nasal Cooling and Sensory Impairments Driving Patient Symptoms With Septal Deviation. *The Laryngoscope*, 132(3):509–517, 2021.

[21] H Nakano, K Mishima, Y Ueda, A Matsushita, H Suga, Y Miyawaki, T Mano, Y Mori, and Y Ueyama. A new method for determining the optimal CT threshold for extracting the upper airway. *Dentomaxillofacial Radiology*, 42(3):26397438, March 2013.

[22] C. Othmer. A continuous adjoint formulation for the computation of topological and surface sensitivities of ducted flows. *International Journal for Numerical Methods in Fluids*, 58(8):861–877, November 2008.

[23] C. Pinter, A. Lasso, and G. Fichtinger. Polymorph segmentation representation for medical image computing. *Computer Methods and Programs in Biomedicine*, 171:19–26, April 2019.

[24] M. Quadrio, C. Pipolo, S. Corti, R. Lenzi, F. Messina, C. Pesci, and G. Felisati. Review of computational fluid dynamics in the assessment of nasal air flow and analysis of its limitations. *European Archives of Oto-Rhino-Laryngology*, 271(9):2349–2354, 2014.

[25] T Radulesco, L. Meister, G. Bouchet, A. Varoquaux, J. Giordano, J. Mancini, P. Dessi, P. Perrier, and J. Michel. Correlations between computational fluid dynamics and clinical evaluation of nasal airway obstruction due to septal deviation: An observational study. *Clinical Otolaryngology*, 44(4):603–611, 2019.

[26] M. Ramanathan, P. Ramesh, N. Aggarwal, A. Parameswaran, H. F. Sailer, and A. E. George. Evaluation of airflow characteristics before and after septoplasty in unilateral cleft patients with a deviated nasal septum: A computational fluid dynamics study. *International Journal of Oral and Maxillofacial Surgery*, 50(4):451–456, April 2021.

[27] J. S. Rhee, D. T. Book, M. Burzynski, and T. L. Smith. Quality of Life Assessment in Nasal Airway Obstruction. *The Laryngoscope*, 113(7):1118–1122, July 2003.

[28] D.G. Roblin and R. Eccles. What, if any, is the value of septal surgery? *Clinical Otolaryngology and Allied Sciences*, 27(2):77–80, April 2002.

[29] Andrea Schillaci. Modellazione e ottimizzazione del flusso nelle cavità nasali. Master thesis, Politecnico di Milano, 2017.

[30] M. Schramm, B. Stoevesandt, and J. Peinke. Optimization of Airfoils Using the Adjoint Approach and the Influence of Adjoint Turbulent Viscosity. *Computation*, 6(1):5, March 2018.

[31] O. Soto and R. Lohner. On the Boundary Computation of Flow Sensitivities. In *42nd AIAA Aerospace Sciences Meeting and Exhibit*, Reno, Nevada, 2004.

[32] C. Sundh and O. Sunnergren. Long-term symptom relief after septoplasty. *European Archives of Oto-Rhino-Laryngology*, 272(10):2871–2875, October 2015.

[33] C. L. N. Tsang, T. Nguyen, T. Sivesind, and A. Cervin. Long-term patient-related outcome measures of septoplasty: A systematic review. *European Archives of Oto-Rhino-Laryngology*, 275(5):1039–1048, January 2018.

[34] T. Udaka, H. Suzuki, T. Kitamura, T. Shiomori, N. Hiraki, T. Fujimura, and N. Ueda. Relationships Among Nasal Obstruction, Daytime Sleepiness, and Quality of Life:. *The Laryngoscope*, 116(12):2129–2132, December 2006.

[35] D. M. Wootton, H. Luo, S. C. Persak, S. Sin, J. M. McDonough, C. R. Isasi, and R. Arens. Computational fluid dynamics endpoints to characterize obstructive sleep apnea syndrome in children. *Journal of Applied Physiology*, 116(1):104–112, January 2014.

[36] Q. Xiao, A. J. Bates, R. Cetto, and D. J. Doorly. The effect of decongestion on nasal airway patency and airflow. *Scientific Reports*, 11(1):14410, July 2021.

[37] G. X. Xiong, J. M. Zhan, H. Y. Jiang, J. F. Li, L. W. Rong, and G. Xu. Computational Fluid Dynamics Simulation of Airflow in the Normal Nasal Cavity and Paranasal Sinuses. *American Journal of Rhinology*, 22(5):477–482, September 2008.

[38] D. Zwicker, K. Yang, S. Melchionna, M. P. Brenner, B. Liu, and R. W. Lindsay. Validated reconstructions of geometries of nasal cavities from CT scans. *Biomedical Physics & Engineering Express*, 4(4):045022, June 2018.

Abstract in lingua italiana

Tra le principali cause anatomiche di ostruzione delle vie aeree superiori le deviazioni settali sono quelle caratterizzate da una maggiore incidenza. In tali casi, con l'obiettivo di alleviare il malessere dei pazienti, i chirurghi otorinolaringoiatri eseguono operazioni di settoplastica funzionale. Tuttavia, nel momento in cui si considera l'effettiva soddisfazione dei pazienti in termini di ripristino di normali funzionalità respiratorie, la percentuale di successo di tali interventi è al di sotto dell'80% . Questa inefficienza della pratica chirurgica è da attribuire all'assenza di uno strumento standardizzato in grado di valutare in maniera quantitativa, e affidabile gli effetti dell'ostruzione stessa. Il presente lavoro pone le basi per lo sviluppo di un metodo innovativo, basato sull'uso della CFD, capace di aiutare i chirurghi otorinolaringoiatri durante la fase di pianificazione dell'intervento di settoplastica. Questo strumento è sviluppato integrando la normale simulazione del flusso d'aria all'interno delle cavità nasali con l'applicazione della formulazione aggiunta usata per calcolare i valori delle derivate di sensitività per un problema di ottimizzazione di forma. La procedura è stata testata su tre diverse anatomie che presentano deviazioni settali di diversa tipologia e severità. Prima di tutto l'effettiva anatomia nasale è ricostruita a partire dalle immagini TC a disposizione. In seguito si simula l'effettivo flusso d'aria ed infine i risultanti campi di velocità e pressione sono usati per avviare la formulazione aggiunta. La mappa di sensitività superficiale ottenuta in questo modo da informazioni su quanto uno spostamento di un punto sulla parete nasale porta benefici in termini di minimizzazione di una funzione obiettivo che simula la resistenza dell'aria. In tutti e tre i casi analizzati lo strumento proposto è stato in grado di identificare tutte le anomalie. I risultati sono stati verificati con l'aiuto di chirurghi che hanno confermato la fattibilità di tutte le correzioni suggerite.

Parole chiave: deviazioni settali, settoplastica funzionale, CFD, formulazione aggiunta, paziente-specifica

Acknowledgements

First I would like to thank those who have made their contribution to the implementation of this paper. I would like to express my heartfelt thanks to Professor Quadrio for its constant support, its dedication to teaching and for giving me the opportunity of exploring a field I have always been interested in. My gratitude goes also to Professor Trimarchi and Doctor Tanzini whose competences have been vital for the realization of this work and who have always been proactive in sharing their knowledge with me. I also thank Ing. Schillaci who was always ready to answer my several questions regarding the technical aspects of the procedure.
My deepest gratitude goes to all members of my family who have been there for me with their love and support. Above all I would like to thank Gaia, Edo and Fede who were always a happy note during these years of study. Last but not least I would like to thank all my friends who have shared this experience with me both at university and when I was back home. These five years would have been much more difficult without you.
Alone you can certainly go faster but together you can definitely go farther.